J Mater Sci (2011) 46:6609–6617
DOI 10.1007/s10853-011-5610-9

Poly(methyl methacrylate)-TiO_2 nanocomposite obtained by non-hydrolytic sol–gel synthesis

D. Morselli · M. Messori · F. Bondioli

Received: 28 January 2011 / Accepted: 4 May 2011 / Published online: 19 May 2011

Abstract Poly(methyl methacrylate) (PMMA)/titanium dioxide (TiO_2) nanocomposites were prepared by means of in situ generation of TiO_2 through a non-hydrolytic sol–gel process (NHSG), starting from titanium chloride, as titania precursor, benzyl alcohol, as oxygen donor, and commercial PMMA. TiO_2 nanoparticles (average size of 30 nm) were obtained in the anatase and amorphous forms. The in situ generation led to a very homogeneous distribution of particulate fillers within the polymeric matrix avoiding the problems related to distributive and dispersive mixing of conventional compounding methods (top down approach). A slight increase of glass transition temperature was observed for all prepared composites with respect to the pristine PMMA. The NHSG process did not affect the molecular weight of the polymers indicating the absence of any degradation reaction for PMMA. The presence of titania in the anatase phase increases the photodegradation of the PMMA matrix due to UV irradiation.

Introduction

Nanoscience and nanotechnology researches have been having a considerable attention in the field of material science, over the last decade. The development of nanocomposite materials, compounded of inorganic fillers embedded in an organic matrix, such as a polymer, is of particular interest in this field. In fact incorporation of inorganic nanoparticles, such as ceramic oxides, into a polymer matrix leads to materials with enhanced properties as compared to both unfilled polymers and polymers filled with micrometric particles. In fact, the presence of fillers is able to change deeply the thermo-mechanical, optical, electrical, and magnetic properties of a polymeric matrix, obviously strongly depending on the nature, shape, size distribution, and crystallinity of the incorporated particles [1–3]. Moreover the use of nano, instead of micro, fillers allows obtaining materials with as good properties as microcomposites but using lower filler concentration, because of the much higher interfacial area between filler and matrix [4]. In bibliography there are many articles on polymeric nanocomposites filled with inorganic oxide nanoparticles and a wide range of synthesis methods are described developing new interesting kinds of materials [5–9]. However, to prepare nanocomposites, it is still widely used the top–down approach, where ex situ preformed nanoparticles are going to be dispersed into the polymeric matrix by physical–mechanical mixing (either melt or solution mixing). Although it is very attractive from an industrial point of view, this method presents some severe limitations related to the difficulties to obtain an effective dispersion and distribution due to the strong tendency of nanoparticles to agglomerate and the significant increase of melt viscosity because of the complex rheology of nanocomposite systems [10]. An interesting alternative technique for the composites preparation without the problems just described is the bottom–up approach. It concerns an in situ generation of filler (generally metal oxides) by a chemical reaction [10], so the filler is synthesized directly within the polymeric matrix.

The sol–gel approach is one of the most employed processes used for this objective. The sol–gel process is a chemical method to prepare inorganic materials, initially employed to synthesize high purity inorganic networks as

D. Morselli · M. Messori (✉) · F. Bondioli
Dipartimento di Ingegneria dei Materiali e dell'Ambiente, Università di Modena e Reggio Emilia, Via Vignolese 905, 41125 Modena (I), Italy
e-mail: massimo.messori@unimore.it

glasses and ceramic materials. Mild conditions characterize this method that becomes strategic when organic materials are involved into the process permitting to avoid their thermal degradation. Typical precursors are metal alkoxides which reacting with water in the presence of an adequate catalyst leads to nanoparticles having narrow grain size distribution with dimensions range between 5 and 100 nm.

The most used method is based on the so-called aqueous sol–gel reaction, which is generally divided into two steps: the first one named hydrolysis, which produces hydroxyl groups, and the second one named condensation, that involves the polycondensation of hydroxyl groups, and residual alkoxyl groups to form a three-dimensional network [11, 12] as follows:

$$\text{Hydrolysis:}\quad M(OR)_x + nH_2O \rightarrow M(OR)_{x-n}(OH)_n + n\text{ROH}$$

$$\text{Condensation:}\quad \equiv M-OH + HO-M\equiv \rightarrow \equiv M-O-M\equiv + H_2O\ (\text{water condensation})$$

$$\text{and/or:}\quad \equiv M-OR + HO-M\equiv \rightarrow \equiv M-O-M\equiv + \text{ROH}\ (\text{alcohol condensation})$$

The presence in the reactive system of an organic oligomer or polymer (bearing or not suitable groups reactive toward to the sol–gel process) leads to the formation of organic–inorganic hybrid structures composed of metal oxide and organic phases intimately mixed each other. The optical, physical, and mechanical properties of these nanocomposites are strongly dependent not only on the individual properties of each component, but also on important aspects of the involved chemistry such as uniformity, phase continuity, domain size, and the molecular mixing at the phase boundaries. The morphologies of the hybrid materials are strictly dependent on the characteristics of the organic polymer such as the molecular weight, the presence and the number of reactive functionalities as well as the solubility of the polymer in the sol–gel system. In despite of these advantages, it is necessary to underlined that the crystallinity of the inorganic phase is generally very low. For this reason, during the last 20 years a lot of researches have been done about the so-called non-hydrolytic sol–gel (NHSG) reaction, to obtain very pure and crystalline silica [13] and other metal oxides, such as V_2O_3, Nb_2O_5, SnO_2, In_2O_3, HfO_2, Ta_2O_5, Ga_2O_3, ZnO, and γ-Fe_2O_3/Fe_3O_4, etc. [14–18].

The NHSG reaction is divided in two steps, as well as the aqueous route. The first reaction step involves either a metal halide or a non-metal halide with an organic oxygen donor (such as alcohols, ether, etc.). The second step, called condensation, can follow different pathways depending on the alkoxide employed. The most important and the most used are the condensations through alkyl halide elimination and/or ether elimination [19–23] as follows:

$$\text{Hydrolysis:}\quad MX_m + n\text{ROH} \rightarrow M(X)_{m-n}(OR)_n + n\text{HX}$$

$$\text{Condensation:}\quad \equiv M-OR + RO-M\equiv \rightarrow \equiv M-O-M\equiv + R-O-R\ (\text{ether condensation})$$

$$\text{and/or:}\quad \equiv M-OR + X-M\equiv \rightarrow \equiv M-O-M\equiv + R-X\ (\text{alkyl}-\text{halide condensation})$$

Regarding titanium dioxide, many articles reported the reaction between titanium chloride and benzyl alcohol [24–27] to obtain pure titanium dioxide crystallized as anatase phase that would not have been possible using the aqueous method that is characterized, as reported, by the obtainment of an amorphous phase. The benzyl group has two functions being able to link the titanium and, at the same time, acts as capping agent and thus as particles size controller.

The in situ generation of titania nanoparticles within a polymer matrix should generate a composite material with improved mechanical and functional properties thanks to the high interfacial interactions present between organic and inorganic phases as a result of the bottom-up approach.

Aim of this study was to obtain a PMMA-TiO_2 nanocomposites through the formation of organic–inorganic hybrid structures using for the first time, to the best of the authors' knowledge, an innovative synthesis method based on NHSG process. This is a preliminary feasibility study on the possibility to obtain a composite material employing NHSG technique with a polymer dissolved into the solvent that acts as well as oxygen donor. In addiction, the presence of oxygens in the PMMA chains are able to bond the TiO_2 nanoparticles through polar interaction between the oxygens and to lead a better connection between inorganic filler and organic matrix leading better mechanical proprieties.

The synthesis was performed at two different temperatures (70 and 100 °C) and with different nominal filler concentrations (5 and 10 wt%) in order to evaluate their effect on reactivity and hybrid microstructure, respectively. Moreover the properties of the obtained materials were evaluated in order to study the effect of the inorganic phase on the polymeric matrix also in comparison with nanocomposites obtained with a commercial nanoparticles by a top-down approach. In particular the effect of photo-active titania nanoparticles on the polymeric matrix used for the preparation of the composite was investigated.

Experimental

Chemicals

Titanium (IV) chloride ($TiCl_4$), benzyl alcohol (BzOH), and methanol (MeOH) were purchased from Sigma-Aldrich (Milan, Italy). Poly(methyl methacrylate) (PMMA, Optixâ CA-1000 I Clear) commercial grade was obtained by Plaskolite West Inc., California (melt flow rate at 230 °C/3.8 kg of 2.3 g/10 min). All chemicals were used as received without further purification expect for BzOH, which was distilled just prior use.

Materials preparation

PMMA-TiO_2 nanocomposites were obtained by NHSG process with a nominal titania concentration of 5 and 10 wt%. To evaluate the effect of temperature on condensation rate, crystallinity and grain size distribution of inorganic phase, the synthesis were conducted at 70 and 100 °C. A typical preparation was as follows: 10 g of PMMA were dissolved in 100 mL of BzOH at around 70 °C. After the dissolution the correct amount of $TiCl_4$ was added drop wise at room temperature under vigorous stirring. The reaction was left stirring at room temperature for 15 min and then reheated to the chosen temperature for 24 h.

The obtained suspension (titania suspended in the PMMA solution in BzOH) was precipitated drop by drop in 500 mL of iced MeOH under vigorous stirring. The precipitated composite flakes were filtered and carefully washed twice with MeOH and then dried at room temperature for 12 h and at 85 °C in an electric oven for 5 h. Finally the composite was dried under vacuum at 170 °C for 3 h to eliminate the residual BzOH.

To better characterize the inorganic phase, titanium dioxide was synthesized in the same condition without the PMMA addition at both previously mentioned temperatures.

To compare the final properties of the obtained materials, a composite was prepared in the same experimental condition but using an ex situ synthesis. After the PMMA dissolution the correct amount of a commercial titanium dioxide (kindly provided by Colorobbia Italia) was added to obtain a 5 wt% composite. The obtained suspension was stirred for 30 min and sonicated for 1 h. The composite was precipitated, purified, and dried using the same procedure used before for the in situ composites.

A list of the prepared particles and composites is reported in Table 1.

TiO_2 powders characterization

The synthesized titania powders and the utilized commercial titania were analyzed with a computer-assisted conventional Bragg–Brentano diffractometer using the Ni-filtered CuKα monochromatic radiation ($\lambda = 1.5418$ Å) (PW3710 Philips) to identify the crystalline phase. The X-ray diffraction (XRD) patterns were collected at room temperature in a 2θ range of 20–60°, with a scanning rate of 0.005°/s and a step size of 0.02°.

Quantitative analysis of the titania samples was performed by the combined Rietveld–RIR (Reference Intensity Ratio) method. A 10 wt% of corundum (NIST SRM 674a annealed at 1500 °C for 1 d to increase crystallinity to 100 wt%) was added to all samples as internal standard. The mixtures, ground in an agate mortar, were side-loaded in an aluminum flat holder in order to minimize the preferred orientation problems. Data were recorded in the 2θ range of 5–140° (step interval 0.02° and 6 s counting time for each step). The phase fractions extracted by the Rietveld–RIR refinements, using GSAS and EXPGUI [28, 29], were rescaled on the basis of the absolute weight of the corundum originally added to the mixtures as an internal standard, and therefore internally renormalized.

Particles morphology was examined by transmission electron microscopy, JEM 2010 TEM (Jeol, Japan). A drop

Table 1 Synthesis conditions of the obtained particles and composites

Sample code	Description
T_C	Commercial TiO_2
T70	TiO_2 synthesized by NHSG at 70 °C
T100	TiO_2 synthesized by NHSG at 100 °C
PMMA_0	PMMA solved in benzyl alcohol and precipitated into cold methanol
PMMA_5T70	PMMA/TiO_2 composite obtained by in situ generation of TiO_2 (nominal content 5 wt%) at 70 °C
PMMA_10T70	PMMA/TiO_2 composite obtained by in situ generation of TiO_2 (nominal content 10 wt%) at 70 °C
PMMA_5T100	PMMA/TiO_2 composite obtained by in situ generation of TiO_2 (nominal content 5 wt%) at 100 °C
PMMA_10T100	PMMA/TiO_2 composite obtained by in situ generation of TiO_2 (nominal content 10 wt%) at 100 °C
PMMA_5T_C	PMMA/TiO_2 composite obtained by solution mixing with preformed TiO_2 nanoparticles (TiO_2 content 5 wt%)

of the obtained suspensions was placed on a copper grid covered with a transparent polymer, followed by drying.

Titanium dioxide particles size distribution analysis was performed directly on the reaction suspension by dynamic light scattering (DLS, Malvern-Zetasizer nano series).

The specific surface area (SSA) and density of the powders were determined by the BET method [30] (Gemini 2360 apparatus, Micromeritics, Norcross, GA, USA) and by a picnometer (Accupic 1330 apparatus, Micromeritics, Norcross, GA, USA), respectively. The particles size was also calculated by Eq. 1, using SSA and density data previously carefully measured:

$$\Phi = 6/(S\rho) \quad (1)$$

where Φ is the average diameter of the spherical particle, S and ρ are, respectively, the experimental SSA and the experimental real density of the obtained powders [31].

The photocatalytic activity of the synthesized powders was evaluated by methylene blue (MB, as molecule model) dye decomposition. 0.01 g of TiO_2 powder was added to 75 mL of 3×10^{-5} M aqueous solution of MB. The suspensions were left under magnetic stirring in a dark chamber for 24 h and then were irradiated for different intervals of time. UV light with wavelength range 325–390 nm and light intensity 5.5 mW/cm^2 was used as light source (Hamamatsu Lightningcure LC8, $\lambda = 300$–450 nm). The color disappearing of the dyes solution was monitored by a UV–vis spectrophotometer (Perkin-Elmer, Lambda 19) in the range 400–800 nm evaluating the absorbance variation at 664 nm. Calibration based on Lambert–Beer law was used to quantify the dye concentration. The photodegradation of MB was calculated by Eq. 2:

$$\text{Photodegradation} = (C_0 - C_t)/C_0 \quad (2)$$

where C_0 is the starting MB concentration and C_t is the MB concentration at t time.

PMMA-TiO_2 composites characterization

To evaluate both the titania reaction yield of sol–gel reaction and the effective titania content in the composites, a gravimetric analysis was performed before and after combustion of the organic matrix in an electric furnace (Optolab-FS5) at 800 °C.

Composites microstructure was investigated by field emission scanning electron microscopy (FESEM, Carl Zeiss-Supra 40) using an over chromium-coated (5 nm) on the fractured surfaces.

The polymer molecular weight was measured by gel permeation chromatography (GPC) using chloroform as eluent (elution rate of 0.3 mL/min) on a HPLC Pump Waters 1515 equipped with a refractive index detector Waters 2410 and a PL gel Mixed-D column.

Dynamic-mechanical characterization was carried out by dynamic-mechanical thermal analyzer (Rheometric Scientific-DMTA 3E) with a single cantilever bending frame geometry.

First, to evaluate the limits of linear viscoelastic, a strain sweep test (at 25 °C) was performed on neat PMMA (specimen dimension 22×6 mm^2). All samples were analyzed from −50 to 160 °C with a heating rate of 3 °C/min, an oscillatory frequency of 1 Hz and a deformation of 0.025%. The bars were prepared by injection moulding using a Minimax Moulder (Custom Scientific Instruments) at 280 °C.

UV radiation exposure tests were carried out on DMTA specimens by using an Osram Ultravitalux UV 300 W lamp. The distance between specimens and lamps was about 18 cm and was set in order to obtain an irradiation intensity of around 5.3–5.5 mW/cm^2 on the samples surface. The effect of the photodegradation was evaluated by FT–IR analysis and by measuring both gloss and weight losses as a function of the irradiation time. FT–IR analysis was performed on the exposed surface of the irradiated specimens with an Avatar 330 FT–IR Thermo Nicolet spectrometer with a ZnSe crystal in ATR mode. A minimum of 32 scans with a resolution of 2 cm^{-1} was used. Gloss measurements were performed on the exposed surface of the irradiated specimens by a Novo Gloss Trio apparatus; measurements were performed by using 60° as standard geometry.

Results and discussion

TiO_2 powders characterization

XRD patterns of T_C and T70 (chosen as representative) were reported in Fig. 1, which shows that both powders are composed by anatase (JCPDS file 01-075-1537) as crystalline phase.

In Fig. 1 it is clearly showed that the investigated powders had a different crystallinity and grain size distribution as underlined by the different peaks intensity and broadening. To quantify the amorphous phase in the powders, Rietveld–RIR analysis was performed (Fig. 2, T70 as representative). Table 2 shows that, as expected, the NHSG synthesis led to powders with a higher degree of crystallization in comparison to aqueous sol–gel synthesized powders as reported elsewhere [32]. In particular, as the temperature is increased there was a slight increase of the anatase phase with respect to the amorphous phase. It is worth noting that T_C, even if not completely crystallized, had a higher anatase content with respect to both synthesized powders.

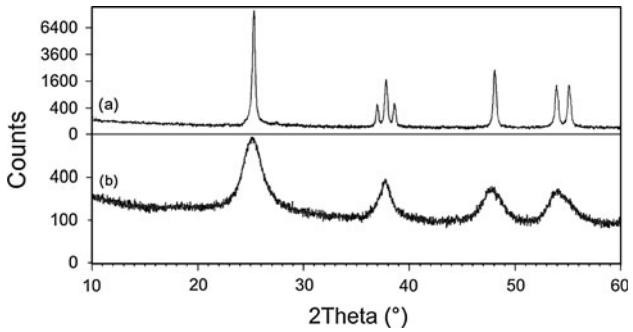

Fig. 1 XRD patterns of T_C (*a*) and T70 (*b*) powders (as representative)

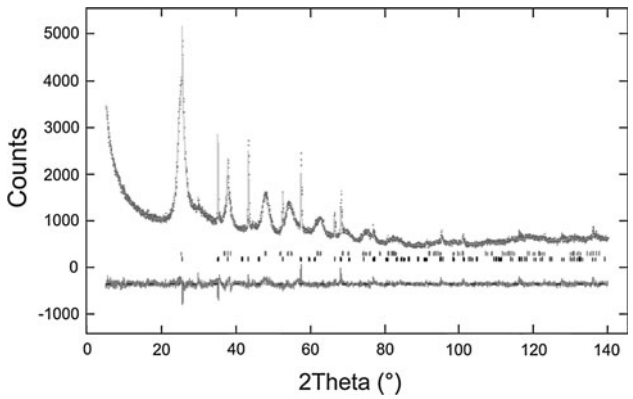

Fig. 2 Rietveld–RIR fit for the T70 pattern (as representative)

TEM and SEM micrographs revealed that T70 and T100 powders were characterized by nanometric crystals of about 25–30 nm (Fig. 3) tightly connected to one another. The obtained results are in good agreement with DLS results (Table 2) that showed the narrow grain size distribution of the obtained nanometric powders. Regarding the commercial powder T_C, the DLS analysis showed a monomodal sub-micrometric grain size distribution and a significantly higher value of average diameter.

The catalytic activity of the obtained powders was determined studying the degradation of MB taking into account also its non-catalyzed degradation due to UV-light. In particular, the MB photodegradation (%) as a function of UV irradiation time with and without T70 is reported in Fig. 4 from which a significant catalytic activity of the titania powder can be deduced. T70 powder was able to promote, in the used UV irradiation condition, a complete photodegradation of MB in about 8 h while in non-catalyzed condition a photodegradation lower than 90 wt% was determined after 24 h.

PMMA-TiO_2 composites characterization

The actual filler content was evaluated for each sample by thermogravimetric analysis and the results are shown in Table 3. The actual titania concentration of in situ generated composites was always significantly lower than the expected values with a maximum yield of about 45% for PMMA_10T100. The relatively low yield in titania could be either attributed to an incomplete (chemical) conversion of $TiCl_4$ precursor to TiO_2 and/or to a partial particles loss during the precipitation, filtration (physical) and washing, procedure adopted to collect the composites. The filtered fraction after precipitation evidenced the presence of a negligible amount of solid residue.

The sol–gel reaction yield without PMMA dissolved, for both temperatures, is almost the same and very high, respectively, for T70 is around 90% and for T100 is around 84% it means that the reaction yield deeply changes when a polymer is dissolved into the solvent. The low sol–gel reaction yield when PMMA is dissolved into the solvent is definitely linked to the composite purification step (precipitation, filtration, and washing); in fact some preliminary tests with longer reaction time were performed and the yields did not change any longer, both with and without PMMA dissolved, after 24 h. It suggests that it is not a kinetic problem and the reaction reaches the chemical equilibrium, but it can justify just a part of yield loss. The different yield at 100 °C is higher than at 70 °C, for both filler concentrations (when PMMA is dissolved) it means that something else affects the reaction yield. For example, it could be affected by the reaction equilibrium *K*, which is affected too by the reaction temperature. Probably, when the temperature gets higher also the yield proportionally increases. It is supported by the constant increase of the percentage yield in titania in comparison to the nominal concentration between samples synthesised at 70 and 100 °C (Table 3).

In order to evaluate possible degradation effects on the polymer during the in situ generation of titania due to the evolution of aggressive chemicals such as hydrochloric

Table 2 Rietveld–RIR results, grain size distribution as determined by DLS data and reaction yield of titania powders

Sample code	Amorphous (wt%)	Anatase (wt%)	χ^2	Rwp	Rp	Reaction yield (%)	d_{50} (nm)
T_C	31.1 ± 0.1	68.9 ± 0.1	4.2530	0.0800	0.0601	/	600 ± 35
T100	57.3 ± 0.2	42.7 ± 0.2	2.5660	0.0561	0.0414	84	30 ± 4
T70	61.2 ± 0.1	38.8 ± 0.1	3.3030	0.0645	0.0464	90	33 ± 8

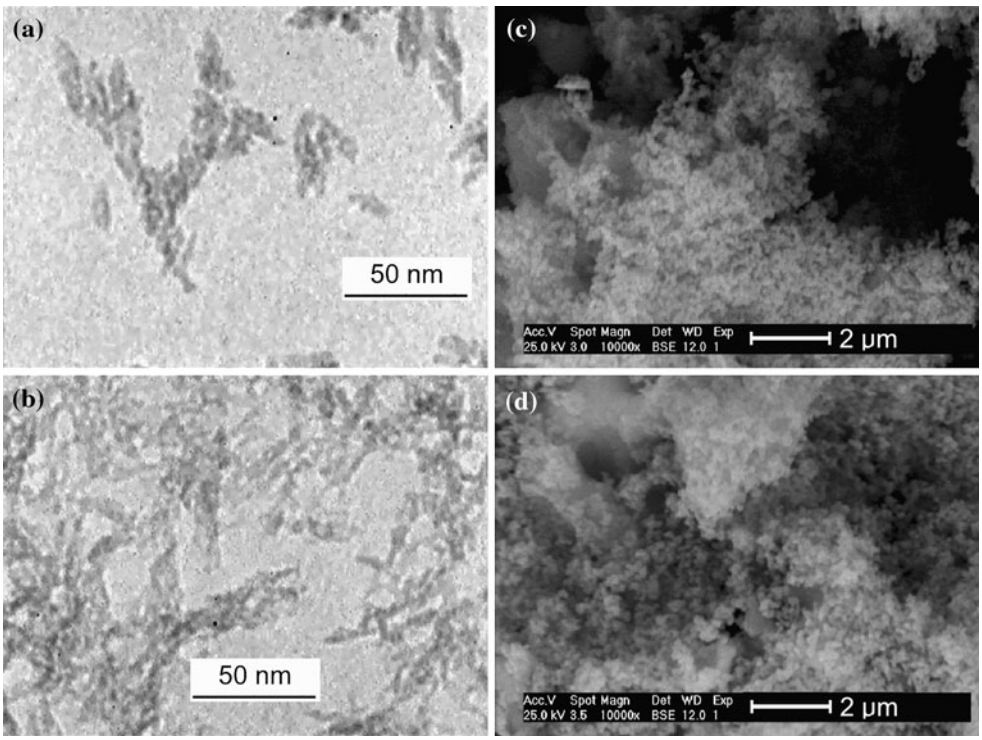

Fig. 3 TEM and SEM micrographs of T70 (**a** and **c**) and T100 (**b** and **d**) samples

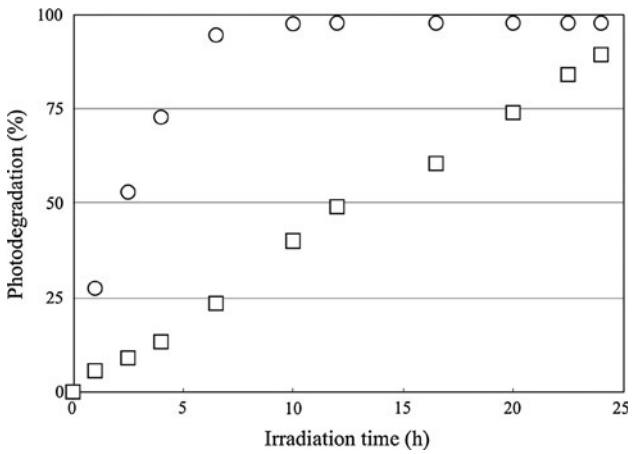

Fig. 4 Methylene blue degradation (%) as a function of UV irradiation time with (*circle*) and without (*square*) T70 powder

acid and other by-products, the molecular weight, and molecular weight distribution were evaluated by GPC for all prepared composites and PMMA_0 samples. GPC traces (here not reported) showed a complete overlapping for all the samples. The overlapping of the GPC traces indicates that the in situ generation of titania from $TiCl_4$ did not affect the molecular weight and molecular weight distribution of the polymer demonstrating the absence of significant degradation reactions during the synthesis.

Table 3 Nominal and actual TiO_2 concentration and glass transition temperature of the prepared materials

Sample code	Nominal TiO_2 concentration (wt%)	Actual TiO_2 concentration (wt%)[a]	T_g (°C)
PMMA_0	–	–	122
PMMA_5T70	5	0.54 ± 0.03 (11%)	124
PMMA_10T70	10	1.68 ± 0.07 (17%)	127
PMMA_5T100	5	1.49 ± 0.16 (30%)	126
PMMA_10T100	10	4.49 ± 0.36 (45%)	126
PMMA_5T_C	5	5.04 ± 0.29 (101%)	126

[a] The percentage yield in titania with respect to the nominal concentration is reported in *brackets*

Glass transition temperature values are reported in Table 3. As expected, T_g increased from 122 °C for unfilled PMMA to about 126–127 °C for samples containing both titania in situ generated and titania mechanically mixed evidencing a slight stiffening effect due to the presence of rigid fillers within the polymeric matrix. It is worth noting the absence of a clear correlation between the amount of titania and the T_g values.

The FESEM micrographs of the fracture surface of PMMA-based composites are reported in Fig. 5. A very rough fracture surface was present in all the investigated samples and the same matrix morphology was also observed for neat PMMA_0 (micrograph here not

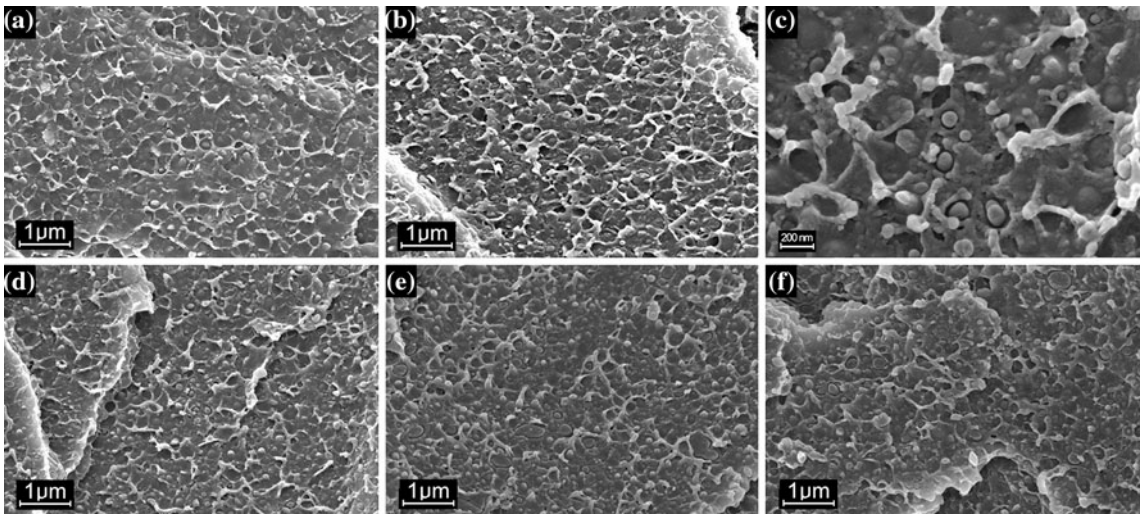

Fig. 5 FESEM micrographs of the fracture surface of **a** PMMA_5T_C, **b** PMMA_5T70, **c** PMMA_5T100 (higher magnification), **d** PMMA_5T100, **e** PMMA_10T70, and **f** PMMA_10T100

reported). Morphology characterized by the presence of very well-distributed particles having spherical shape and maximum diameter less than 100 nm (see in particular Fig. 6c, taken at higher magnification) was observed for all the composites. The chemical composition of the particles was consistent with the expected titania as indicated by energy dispersive X-ray spectrometry (EDS). FESEM analysis indicated that the NHSG method was an effective process to obtain nanocomposite materials with an effective dispersion and distribution of nanoparticles avoiding significant particles agglomeration and melt viscosity increase. It is important to note that the titania particles diameter of PMMA_5T_C showed by FESEM analysis was in disagreement with the values obtained by DLS analysis suggesting the presence of aggregation phenomena during the DLS analysis itself.

In order to evaluate the effect of the titania on the PMMA photodegradation, specimens were placed in a black chamber, and irradiated with UV light for several hours (up to 1200 h). FT–IR spectra recorded in ATR mode for exposed surfaces of PMMA with and without titania filler are reported in Figs. 6 and 7 together with the spectrum of pure titania powder. FT–IR/ATR spectra of PMMA_0 before and after 1200 h of UV irradiation (Fig. 6) are substantially overlapped indicating the absence of surface chemical modification and thus significant degradation. On the contrary, the presence of titania particles led to a significant modification of the FT–IR/ATR spectra as a result of UV irradiation. In particular the ratio between signals, respectively, attributable to PMMA and titania decreased significantly after UV irradiation (compare Fig. 7, spectra a–b taking into account to the spectrum of

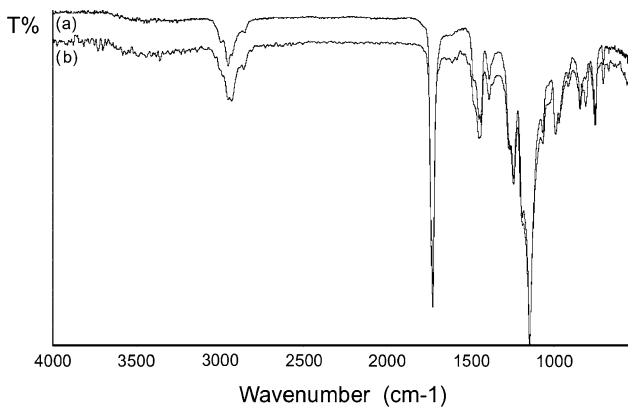

Fig. 6 FT–IR spectra of PMMA_0 before (*a*) and after (*b*) UV irradiation (irradiation time 1200 h)

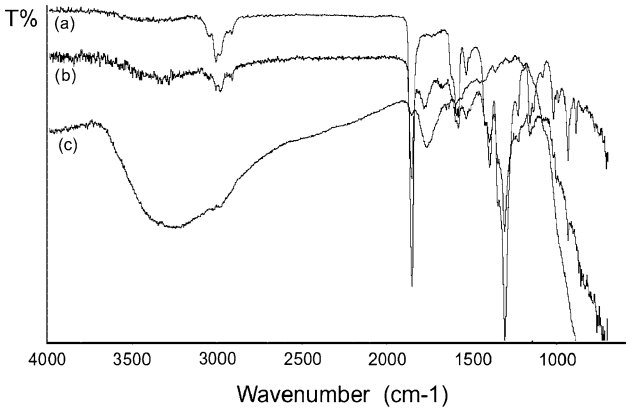

Fig. 7 FT–IR spectra of PMMA_10T70 before (*a*) and after (*b*) UV irradiation (irradiation time 1200 h) and of T70 (*c*)

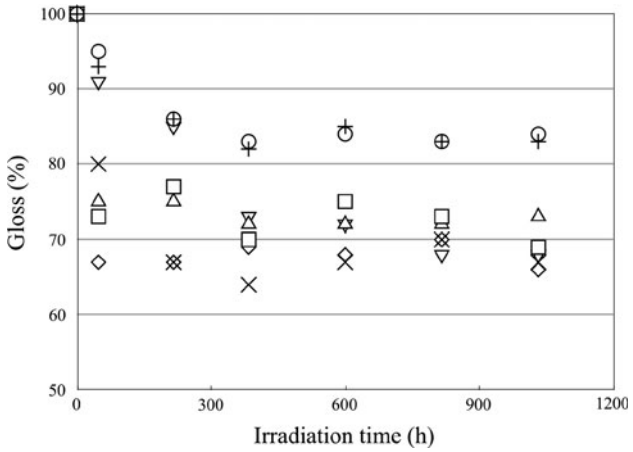

Fig. 8 Percent gloss (relative to the initial value) as a function of UV irradiation time (*plus* PMMA_c; *circle* PMMA_0; *square* PMMA_5T70; *times* PMMA_5T100; *triangle* PMMA_10T70; *diamond* PMMA_10T100; *inverted diamond* PMMA_5T_C)

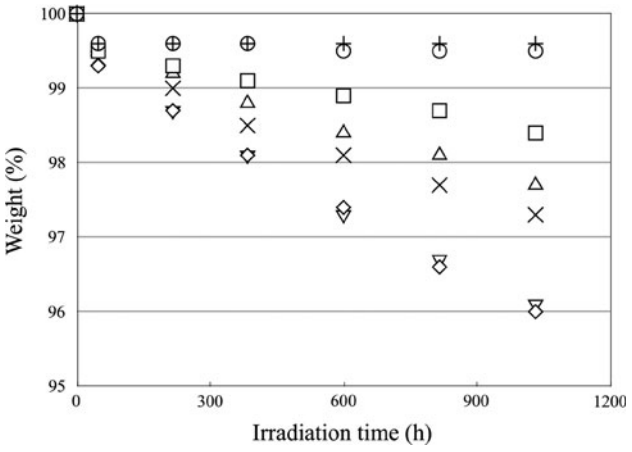

Fig. 9 Percent weight (relative to the initial value) as a function of UV irradiation time (*plus* PMMA_c; *circle* PMMA_0; *square* PMMA_5T70; *times* PMMA_5T100; *triangle* PMMA_10T70; *diamond* PMMA_10T100; *inverted diamond* PMMA_5T_C)

pure titania in Fig. 9, spectrum c). These results can be described taking into account the well-known degradation mechanism for PMMA that leads to the decomposition of the polymer and the formation of volatile by-products. In this way, the strong modification of FT–IR/ATR spectra can be explained as a sort of surface 'erosion' of the PMMA induced by the UV irradiation that increases the surface concentration of titania with respect to the organic polymer.

Similar effects were observed by measuring the percent gloss and weight (relative to the corresponding initial values) as a function of the irradiation time (Figs. 8 and 9).

Concerning gloss measurements, which can be considered as an evaluation of surface roughness increase after erosion due to PMMA photodegradation, all samples showed a significant decrease in gloss in the early stages of irradiation (after 50 h for filled PMMA and after 200 h for unfilled PMMA) followed by substantially constant values for higher irradiation times. Only PMMA_5T_C represented an exception with a progressive and almost linear decrease of gloss during all the investigated irradiation time range. In agreement with the above discussed FT–IR/ATR data, the presence of in situ generated titania enhanced the decrement of the gloss as evidenced by the plateau values: 83–84% for unfilled PMMA (PMMA_c and PMMA_0), 67–73% for PMMA filled with titania (PMMA_5T70, PMMA_5T100, PMMA_10T70, PMMA_10T100).

Taking into account the degradation mechanism of PMMA (polymer decomposition with formation of low molecular weight by-products and their volatilization), a further possibility for the investigation of photodegradation effects could be represented by the specimen weight loss during UV irradiation. Data reported in Fig. 9 indicated that the weight loss for unfilled PMMA was almost negligible (less than 0.5%). On the contrary, all the samples containing titania exhibited a significant and linear mass decrease over the entire irradiation time range. It is very interesting to observe that the slopes of the curves increased by increasing the actual TiO_2 concentration (see Table 3) indicating the crucial role played by the amount of titania in the photodegradation reaction. It is also very fascinating that the curves corresponding to different samples prepared by in situ generation or mechanical mixing of titania but with very similar titania content (PMMA_10T100 and PMMA_5T_C, with an actual titania concentration of 4.49 and 5.04 wt%, respectively) are perfectly overlapped.

Conclusions

Titania nanoparticles of average size of 30 nm and anatase form were in situ generated within PMMA by means of NHSG process. The particles were uniformly distributed without significant particle–particle aggregation because of the bottom–up approach used for the synthesis. Independent characterization techniques showed that the presence of titania led to an enhancement in the photodegradation phenomena induced by UV irradiation.

References

1. Ajayan PM, Schadler LS, Braun PV (2003) Nanocomposite science and technology. WILEY-VCH, Weinheim
2. Liu T, Burger C, Chu B (2003) Prog Polym Sci 28:5
3. Kickelbick G (2003) Prog Polym Sci 28:83
4. Schmidt G, Malwitz MM (2003) Curr Opin Coll Int Sci 8:103

5. Hamming LM, Qiao R, Messersmith PB, Brinson LC (2009) Compos Sci Technol 69:1880
6. Matsuyama K, Mishima K (2009) J Supercrit Fluids 49:256
7. Ngo VG, Bressy C, Leroux C, Margaillan A (2009) Polymer 50:3095
8. Dzunuzovic E, Jeremic K, Nedeljkovic JM (2007) Eur Polym J 43:3719
9. Convertino A, Leoa G, Tamborra M, Sciancalepore C, Striccoli M, Curri ML, Agostiano A (2007) Sens Actuators B 126:138–143
10. Mittal V, Kim JK (2010) In: Advances in elastomeric nanocomposites. Springer, Berlin
11. Brinker C, Scherer G (1990) Sol-gel science: the physics and chemistry of sol-gel processing. Academic Press, Boston
12. Wen J, Wilkes GL (1996) Chem Mater 8:1667
13. Bourget L, Corriu RJP, Leclercq D, Mutin PH, Vioux A (1998) J Non-Cryst Solids 242:81
14. Niederberger M, Pinna N (2005) Prog Solid State Chem 33:59
15. Pinna N, Antonietti M, Niederberger M (2004) Colloids Surf A Physicochem Eng Asp 250:211
16. Pinna N, Neri G, Antonietti M, Niederberger M (2004) Angew Chem Int Ed 43:4345
17. Pinna N, Garnweitner G, Antonietti M, Niederberger M (2004) Adv Mater 16:23
18. Pinna N, Garnweitner G, Antonietti M, Niederberger M (2005) J Am Chem Soc 127:5608
19. Arnal P, Corriu RJP, Leclercq D, Mutin PH, Vioux A (1997) Chem Mater 9:694
20. Mutin PH, Vioux A (2009) Chem Mater 21:582
21. Corriu R, Leclercq D, Lefevre P, Mutin PH, Vioux A (1992) Chem Mater 4:961
22. Corriu R, Leclercq D, Lefevre P, Mutin PH, Vioux A (1992) J Mater Chem 2:673
23. Corriu R, Leclercq D, Lefevre P, Mutin PH, Vioux A (1992) J Non-Cryst Solids 146:301
24. Niederberger M, Bartl MH, Stucky GD (2002) Chem Mater 14:4364
25. Niederberger M, Garnweitner G, Krumeich F, Nesper R, Cölfen H, Antonietti M (2004) Chem Mater 16:1202
26. Zhu J, Yang J, Bian ZF, Ren J, Liu YM, Cao Y, Li HX, He HY, Fan KN (2007) Appl Catal B Environ 76:82
27. Jia H, Zheng Z, Zhao H, Zhang L, Zou Z (2009) Mater Res Bull 44:1312
28. Larson AC, Von Dreele RB (2000) General structure analysis system (GSAS). Los Alamos National Laboratory Report LAUR: 86-748
29. Toby BH (2001) J Appl Crystallogr 34:210
30. Brunauer S, Emmett PH, Teller E (1938) J Am Chem Soc 60:309
31. Kodera K (1962) Powders (Theory and Applications). Maruzen, Tokyo
32. Bondioli F, Dorigato A, Fabbri P, Messori M, Pegoretti A (2008) Polym Eng Sci 48:448